Three-Dimensional Characterization of the Normal Human Parafoveal Microvasculature Using Structural Criteria and High-Resolution Confocal Microscopy

Dong An,[1,2] Paula Yu,[1,2] K. Bailey Freund,[3,4] Dao-Yi Yu,[1,2] and Chandrakumar Balaratnasingam[1,2,5]

[1]Centre for Ophthalmology and Visual Science, University of Western Australia, Nedlands, Western Australia, Australia
[2]Lions Eye Institute, Nedlands, Western Australia, Australia
[3]Vitreous Retina Macula Consultants of New York, New York, New York, United States
[4]Department of Ophthalmology, New York University School of Medicine, New York, New York, United States
[5]Department of Ophthalmology, Sir Charles Gairdner Hospital, Nedlands, Western Australia, Australia

Correspondence: Dao-Yi Yu, Centre for Ophthalmology and Visual Science, The University of Western Australia, Nedlands, Western Australia 6009, Australia; dyyu@lei.org.au.

Received: February 28, 2020
Accepted: April 30, 2020
Published: August 4, 2020

Citation: An D, Yu P, Freund KB, Yu D-Y, Balaratnasingam C. Three-dimensional characterization of the normal human parafoveal microvasculature using structural criteria and high-resolution confocal microscopy. *Invest Ophthalmol Vis Sci.* 2020;61(10):3. https://doi.org/10.1167/iovs.61.10.3

Purpose. To use structural criteria to reconcile the three-dimensional organization and connectivity of the parafoveal microvasculature.

Methods. The parafoveal microvasculature was perfused and labeled in 16 normal human donor eyes for lectin, alpha smooth muscle actin, and filamentous actin. Established structural criteria gathered using confocal microscopy, including vessel diameter, endothelial cell morphology, and presence/density of smooth muscle cells, were used to differentiate arteries, arterioles, capillaries, venules, and veins. Three-dimensional visualization strategies were used to define the connections between retinal arteries and veins within the superficial vascular plexus (SVP), intermediate capillary plexus (ICP), and deep capillary plexus (DCP).

Results. The parafoveal microvasculature has two different inflow patterns and seven different outflow patterns. The SVP and ICP were connected to retinal arteries by arterioles. Inflow into the DCP occurred only via small arterioles (a1; mean diameter, 8.3 µm) that originated from the ICP. Direct connections between the DCP and retinal arteries were not identified. Each capillary plexus formed its own venule that drained independently or in conjunction with venules from other plexuses into a retinal vein at the level of the ganglion cell layer. For the DCP, a1 was significantly smaller than its draining venule (mean diameter, 18.8 µm; $P < 0.001$).

Conclusions. The SVP and ICP of the parafoveal microvasculature have both in series and in parallel arterial and venous connections. Arterial supply to the DCP originates from the ICP, but with direct drainage to the retinal vein. These findings may help to develop an understanding of the pattern of retinal lesions characterizing a myriad of retinal vascular diseases.

Keywords: retina, macula microvasculature, capillary, αSMA

The immense energy demands of the human macula are satisfied by both the choriocapillaris and the precise and layered arrangement of retinal capillary networks.[1–4] Unlike the choroid and other parts of the central nervous system, the angio-architectural properties of the macula are constrained by a need to optimize its optical properties.[5] A fundamental requisite for the structural arrangement of the macular circulation is that nutrient, waste, and heat exchange can be optimized without interfering with the trajectory of incident lights rays toward the photoreceptor layer. Accurate delineation of the three-dimensional (3D) arrangement of the macular circulation, including arterial inflow pathways, venous outflow pathways, and connections between capillary plexuses, is critical for understanding the vasculogenic processes that support retinal homeostasis and for determining the pathogenic mechanisms that underlie retinal vascular diseases.

Although it is widely agreed that the human retinal circulation can be divided into superficial, intermediate, and deep capillary plexuses,[6–8] there remains some conjecture regarding the morphology, order, and organization of retinal vessels that comprise each of these plexuses. The conduit patterns that connect the different plexuses to arterial and venous systems also has not been resolved. This issue cannot be reliably reconciled using animal models, as most mammals do not manifest a macula featuring a foveal avascular zone. The macular anatomy of non-human primates is comparable to that of humans, but the elegant works by Snodderly and colleagues[9,10] have highlighted important distinctions in the organization of foveal

vasculature between monkey species such as squirrel and macaque, conveying the importance of caution in extrapolating features of the monkey macular circulation in toto to the human eye. Histology coupled with microscopic techniques has facilitated detailed evaluation of fine retinal capillaries, but many studies of the human eye using such methodology have utilized tissue-digestion techniques, thereby making it difficult to clearly define the spatial relationships between capillary plexuses and neural layers.[11–13] These limitations to date have made it challenging to reconstruct the human macular circulation in three dimensions with highly detailed depth-related information.

Optical coherence tomography angiography (OCTA) techniques have facilitated in vivo examination of the human macular microvasculature at an unprecedented level.[14] However, important limitations of OCTA include projection artifacts, motion artifacts, segmentation errors, difficulty in detecting flow parallel to the scanning laser beam, and localized loss of signal strength due to media opacities.[15] The spatial resolution of most commercially available OCTA devices (7–20 µm in axial plane)[16–18] is also generally lower than that of postmortem microscopic techniques, thus making it challenging to differentiate various orders of the arterial and venous circulations using OCTA alone. Furthermore, as OCTA utilizes the principle of motion contrast to visualize a vascular structure,[19] vessels of low flow may not be represented on OCTA slabs, thereby influencing the interpretation of connectivity patterns between capillary plexuses. These collective limitations may be one reason for the discrepancies in the 3D vascular models proposed of the macula by different investigators using OCTA.[20–23]

Previous investigations concerning vascular anatomy and physiology have proposed that a more reliable categorization of vascular systems requires integration of data regarding vascular diameter and the characteristics of perivascular elements such as smooth muscle cells and pericytes.[24–26] Such a construct provides more meaningful inference of the physiologic role and hemodynamic properties of each segment of the vascular system. This report utilizes high-resolution confocal scanning laser microscopy, perfusion-labeled immunohistochemical techniques,[27] and 3D image reconstruction software to characterize the organization of the normal human parafoveal circulation. We utilize established histologic criteria that incorporate information regarding size of vessels, structure of endothelia, and the presence/density of surrounding smooth muscle cells to differentiate arteries, arterioles, capillaries, venules, and veins. A 3D vascular model of the human parafovea is subsequently proposed. The purpose of this study is manifold: (1) it expands our understanding of mechanisms that control blood flow in the human macula, thereby allowing us to speculate upon the pathophysiology of important retinal vascular diseases such as diabetic retinopathy (DR), retinal vein occlusion (RVO), and paracentral acute middle maculopathy (PAMM); and (2) it provides important structural data that refines our interpretation of clinical OCTA images.

Materials and Methods

The study was approved by the human research ethics committee at the University of Western Australia. All human tissue was handled according to the tenets of the Declaration of Helsinki.

Donor Retina Preparation

Human donor eyes used in this report were obtained from DonateLife WA, the organ and tissue retrieval authority in Western Australia, Australia, and the Lions Eye Bank. Eyes were enucleated within 24 hours of death. Eyes were prepared using our previously described techniques.[28,29] In brief, enucleated eyes were transported in oxygenated Ringers lactate solution. The eyes were placed in a custom-built eye holder, and the central retinal artery was cannulated with a glass micropipette for perfusion labeling.[4,8,29,30] The eyes were cannulated using a glass micropipette (100-µm tip diameter) and perfused with the following solutions in sequence at a rate of 60 µL per minute unless otherwise stated: 1% bovine serum albumin in Ringer's solution for 20 minutes; 4% paraformaldehyde in 0.1-M phosphate buffer (PB) for 20 minutes; and 0.1-M PB for 20 minutes. Next, eyes were perfused using one of the following protocols:

- Lectin (endothelial cell membrane labeling)—Perfuse 40 µg lectin–fluorescein isothiocyanate (FITC, L4895; Sigma-Aldrich, St. Louis, MO, USA) and 2.5 µL Hoechst (H6024; Sigma-Aldrich) in 400 µL PB over a period of 30 seconds, left within the vasculature for 12 minutes, and washed out with PB perfusion over 20 minutes. Lectin binds to glycoproteins of cell membranes. With its large molecular weight, minimal vascular extravasation occurs during the perfusion-labeling process, allowing for clear labeling of the vascular luminal endothelium only, which is advantageous for studying 3D vascular networks with minimal background noise interference.[8,29]
- Phalloidin (F-actin labeling)—Perfuse 0.1% Triton X-100 (Sigma-Aldrich) in 0.1-M PB for 5 minutes, followed by 1 µg phalloidin tetramethylrhodamine B isothiocyanate (TRITC, P1951; Sigma-Aldrich) and 2.5 µL Hoechst in 1 mL PB delivered over three 30-second perfusions 20 minutes apart and washed out with PB perfusion over 20 minutes. Phalloidin binds to F-actin molecules and allows visualization of endothelial cell borders. Due to its low molecular weight, phalloidin can diffuse across endothelial cells and, most importantly, enter vascular smooth muscle cells due to their high F-actin content.[25,28]
- Anti-α-smooth muscle actin (αSMA)/lectin colabeling—Full lectin perfusion protocol is followed by 0.1% Triton X-100 in 0.1-M PB for 5 minutes. Then, 20 µL mouse anti-αSMA (A2547; Sigma-Aldrich) and 10 µL 100% donkey serum in 1 mL PB are delivered via three perfusions of 30 seconds, 20 minutes apart, then washed out using PB perfusion over 20 minutes after a total of 1 hour of labeling time. Next, 20 µL of Donkey Anti-Mouse (Alexa Fluor 647, ab150111; Abcam, Cambridge, UK) in 1 mL PB was delivered via three perfusions of 30 seconds, 20 minutes apart, followed by washout using PB perfusion over 20 minutes after 1-hour labeling time. αSMA is an isoform of the actin molecule and can be found in high concentrations within smooth muscle cells and, in particular, arteriole branch sites and pericytes.[31–34]
- Anti-αSMA/phalloidin colabeling—Phalloidin 1 µg was added to the secondary antibody solution of the αSMA protocol.

Investigative Ophthalmology & Visual Science

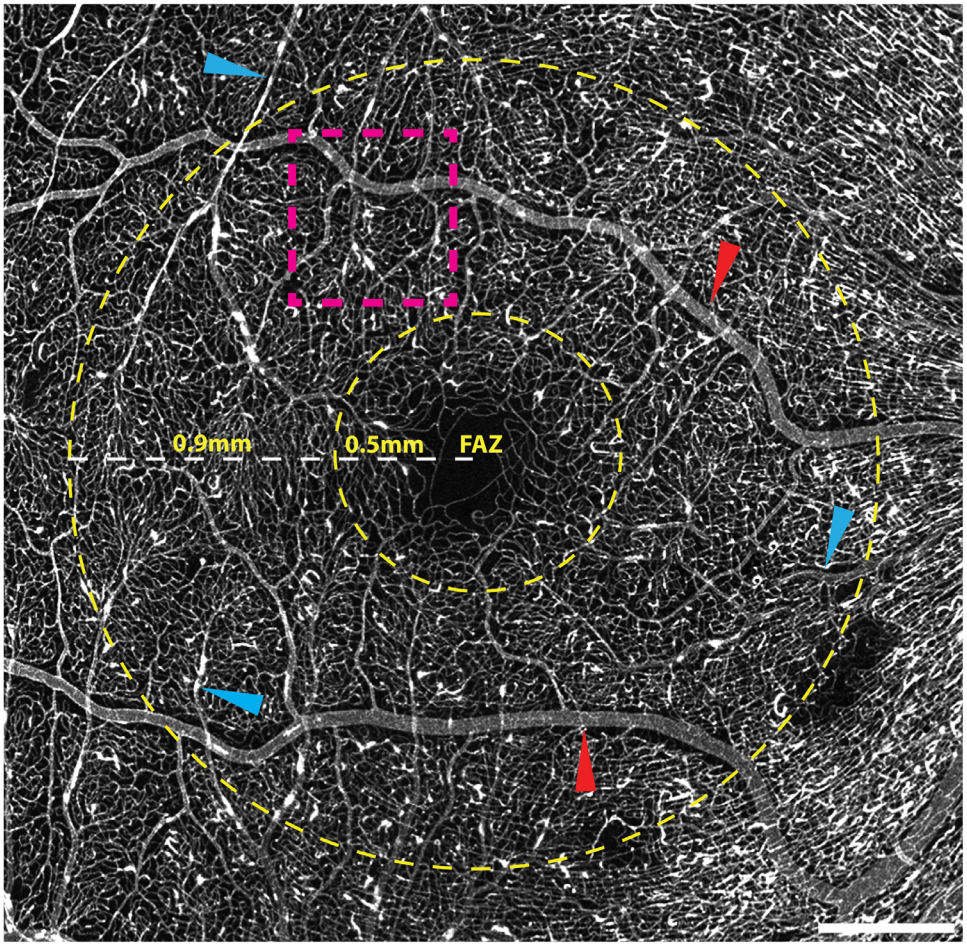

Figure 1. Whole-mount retina montage (donor eye 12, right eye) following perfusion labeling with lectin fluorescein isothiocyanate. The area of interest in this study is the parafovea, denoted by the outer and inner rings located 1.4 mm and 0.5 mm from the center of the foveola, respectively. The *magenta grid* indicates an example of a 0.635 × 0.635-mm sampling field within the study perimeter. *Red arrowheads* point to arteries with a prominent capillary free zone, and *blue arrows* point to veins that have collapsed walls. The retinal peripapillary capillary network can be seen extending into the superotemporal and inferotemporal arcades from the optic disc. FAZ, foveal avascular zone. *Scale bar*: 500 µm.

Post-perfusion, the eyes were decannulated and dissected along the equator. The vitreous was carefully peeled and dissected from the retina. The posterior segment was then immersed in 4% paraformaldehyde for 12 hours. Next, the neuroretina was detached from the retinal pigment epithelium. The optic nerve head was sectioned to be continuous with the retina. The retina was flat mounted on a glass slide by making several radial incisions along the edge. Glycerol (Merck Pty Ltd., Victoria, Australia) was added to enhance the optical quality of the tissue before placement of the coverslip.

Confocal Scanning Laser Microscopy

Macular vasculature was sampled from an area confined by two circular rings as shown in Figure 1. The outer and inner rings were located 1.4 mm and 0.5 mm from the center of the foveola, respectively. The outer ring represents the boundary of the parafovea as previously defined by Hogan et al.[5] Sampling within the inner ring was avoided, as the three macula plexuses converge into a single plexus, terminating at the foveal avascular zone inside this ring.[5]

Retina flat mounts were imaged using a confocal scanning laser microscope (Eclipse 90i and C1; Nikon Corporation, Tokyo, Japan) equipped with four solid-state lasers at wavelengths of 405 nm, 488 nm, 561 nm, and 635 nm. For each retina flat mount, two low magnification images were captured from a random location within the study perimeter using a Nikon Plan Apochromat VC 20X (NA 0.75) dry objective lens, which gave a field of view of 0.635 mm × 0.635 mm. Two higher magnification images were acquired from each αSMA F-actin colabeled retinas using a Nikon 60× oil objective lens with a field of view of 211 µm × 211 µm or Nikon 40× oil objective lens with a field of view of 312 µm × 312 µm to visualize vascular endothelia, pericytes, and smooth muscle cells. The contractile protein distribution within arterioles, capillaries, and venules was also studied. Each stack consisted of a depth of optical sections, 1 µm apart, along the *z*-axis between the vitreous face and the avascular outer nuclear layer. Immunofluorescence labeling using Hoechst (405 nm), lectin FITC (488 nm), phalloidin TRITC (561 nm), and Alexa Fluor 488 Donkey Anti-Mouse (635 nm) were visualized via argon laser excitation with emissions detected through 450-nm, 515-nm, 605-nm, and 668-nm bandpass filters, respectively.

Investigative Ophthalmology & Visual Science

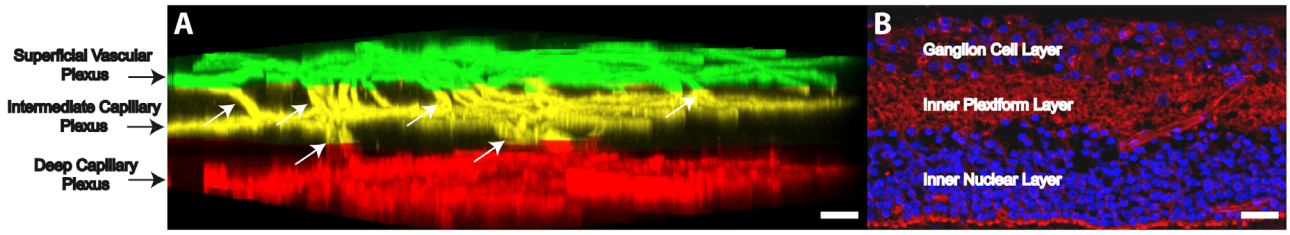

Figure 2. Three-dimensional, full thickness, color-coded retina section labeled with lectin rotated to visualize distinct retinal capillary plexuses and their connections in the parafovea (**A**). The SVP, ICP, and DCP have been false-colored *green*, *yellow*, and *red*, respectively. Note that the interconnections between the SVP and ICP are observably more numerous than those between the ICP and DCP (*arrows*). Cross-section of the parafovea labeled using phalloidin (F-actin) and Hoechst (nuclei) illustrate the depths of retinal capillary plexuses and their position relative to retinal layers (**B**). The SVP is located between the inner limiting membrane and the border of the ganglion cell layer/inner plexiform layer (IPL). The ICP is located between the IPL and inner half of the inner nuclear layer (INL). The DCP is located between the outer half of the INL and the outer plexiform layer. Cryosection color code: *red*, F-actin; *blue*, nuclei. *Scale bar*: 50 µm. Images in **A** and **B** were obtained from different donor eyes.

Image Analysis

Confocal image files were processed with Imaris (Bitplane, Zurich, Switzerland) and ImageJ (National Institutes of Health, Bethesda, MD, USA) software. All images in this manuscript were prepared using Adobe Illustrator CC 2018 22.1 (Adobe Inc., San Jose, CA, USA). Three-dimensional images of each confocal stack were generated and viewed using Imaris software at different angles of rotation. We analyzed confocal 3D stacks to stratify capillary networks, define orders of the vascular tree, and determine patterns of connectivity within the retinal circulation as described under the subheadings below.

Stratification of Retinal Vascular Networks. Morphologic characteristics of capillaries and nuclei position as previously described were used to stratify different vascular/capillary networks within the 3D stack as follows (Fig. 2):[7,21,35,36]

- Superficial vascular plexus (SVP)—Located between the inner limiting membrane and the border of the ganglion cell layer (GCL)/inner plexiform layer (IPL). Some sampling locations also contained peripapillary capillaries,[7] which were considered to be part of the SVP for this study.
- Intermediate capillary plexus (ICP)—Located between the IPL and the inner half of the inner nuclear layer (INL).[7]
- Deep capillary plexus (DCP)—Located within the outer half of the INL and the outer plexiform layer.[7]

For consistency, SVP was false-colored green, the ICP was false-colored yellow, and the DCP was false-colored red in all lectin-labeled figures in this manuscript.

Categorization of Vascular Structures in the Retinal Circulation. Following stratification of the 3D stack into the SVP, ICP, and DCP, we carefully analyzed each vascular structure within the confocal volume and categorized it as artery, arteriole, capillary, venule, or vein. Our categorization of different vascular structures was based on published definitions of endothelial morphology,[4,37,38] smooth muscle cell morphology,[39] and orientation, as well as lumen diameter for artery, arteriole, capillary, venule, and vein.[38] The definitions that were used are as follows (Fig. 3):

- Artery (Figs. 3A, 3B)—As per the definition by Hogan et al.,[39,40] retinal arteries were considered to be vascular structures with a diameter > 15 µm. Retinal arteries were also distinguished by endothelial cells where the nuclei and long axis of the cell were oriented parallel to the direction of blood flow.[38] Intracellular microfilament (stress fibers) were seen as short and thick bundles within endothelial cells of arteries.[38] Arteries were also characterized by a coat of smooth muscle cells (usually one or more layers) that were perpendicularly oriented and circumferentially enveloped the endothelial cells of retinal arteries.[39] Retinal arteries were surrounded by a capillary-free zone that was localized to the SVP.[8]
- Arteriole (Figs. 3C, 3D)—As per the definition by Hogan et al.,[40] retinal arterioles were considered to be vascular structures with a diameter between 8 and 15 µm that adjoined arteries to capillaries. Arterioles were characterized by a surrounding capillary-free zone that was not seen in venules of comparable lumen diameter.[8,40] An arteriole was differentiated from a venule by its thicker wall with a circular pattern of smooth muscle cells (one layer) encircling it.[30]
- Capillary (Figs. 3E, 3F)—These were considered to be vascular structures with a diameter less than 8 µm.[40] Capillaries were characterized by a single layer of endothelium and basement membrane.[7,40,41] Capillary endothelium were characterized by long intracellular microfilament distributions that were oriented parallel to the long axis of the cell, as well as large oval-shaped nuclei that were oriented parallel to the direction of blood flow.[38] In this study, a capillary loop was defined as a fully enclosed two-dimensional structure formed by two or more capillaries located within the same plexus. These capillaries share a common arterial supply and venous drainage.
- Venule (Figs. 3G, 3H)—These were considered to be vascular structures between 8 and 20 µm in diameter that adjoined capillaries to retinal veins.[40,42] The endothelium of venules was similar to that of capillaries.[40]
- Vein (Figs. 3I, 3J)—Vessels larger than 20 µm in diameter that were connected to venules were defined as veins.[39,40] The morphology of venous endothelia was very different from that of arteries, arterioles, and capillaries and demonstrated a polygonal shape

Investigative Ophthalmology & Visual Science

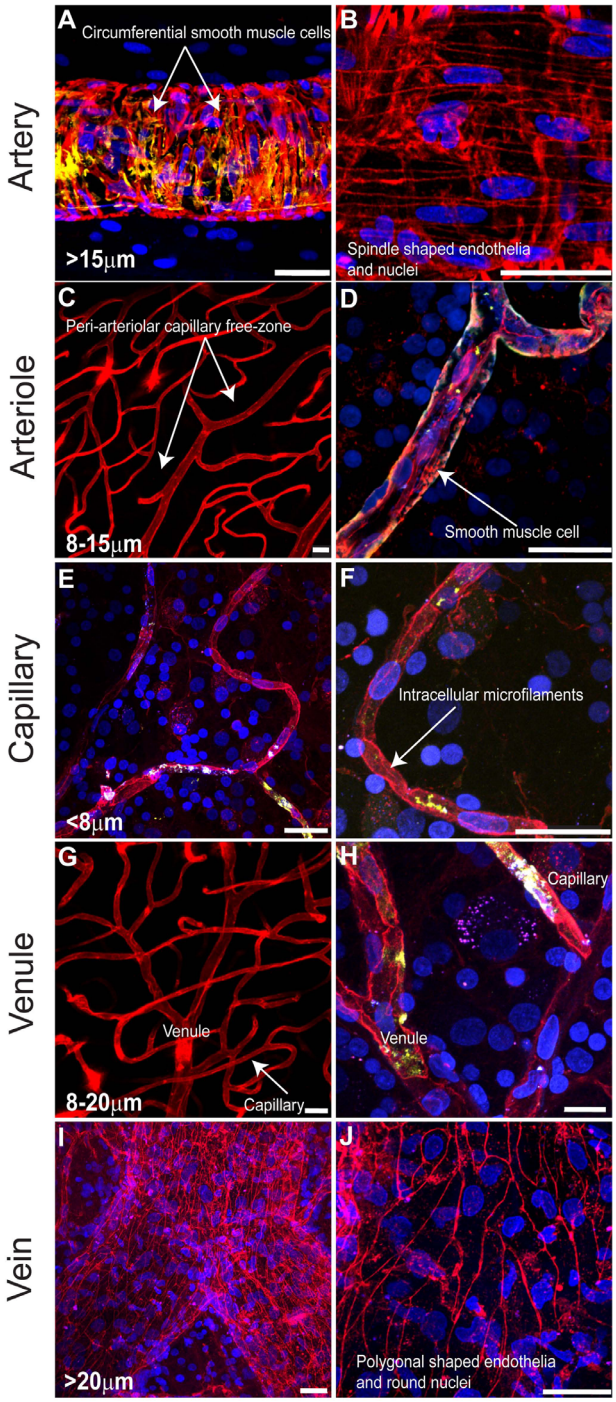

Figure 3. Histologic criteria used to define the parafoveal circulation. Typical characteristics of a retinal artery (**A**, **B**), arteriole (**C**, **D**), capillary (**E**, **F**), venule (**G**, **H**), and vein (**I**, **J**) are presented. Arteries were vessels that were greater than 15 μm in diameter and contained one or more layers of smooth muscle cells arranged in a circumferential pattern with smooth muscle cell nuclei arranged perpendicular to the direction of flow. The spindle-shaped endothelial cells and nuclei of arteries had their long axis arranged parallel to the direction of flow. Arterioles were defined as vessels between 8 and 15 μm in diameter and containing a periarteriolar capillary-free zone that is not as pronounced as in arteries. Smooth muscle cells were sparsely distributed along the walls of arterioles. Capillaries were vessels that were less than 8 μm in diameter and were characterized by endothelial cells with large, oval-shaped nuclei. Venules were vessels between 8 and 20 μm in diameter and did not demonstrate a surrounding capillary-free zone. Venular endothelial cells demonstrated irregularly shaped nuclei. Veins were more than 20 μm in diameter with polygonal-shaped endothelial cells having round nuclei. *Red*, F-actin; *yellow*, αSMA; *blue*, nuclei. *Scale bars*: 30 μm.

with round nuclei.[38] Veins were encircled by only a sparse number of smooth muscle cells that were irregular in shape and orientation.[43]

Defining Vascular Patterns and Connections in the Retinal Circulation. Vascular branching patterns and connections were studied using confocal stacks acquired with a 10× lens. The IMARIS Surpass function was used to visualize the retinal vasculature at different angles of rotation to define inflow and outflow patterns. We studied inflow patterns to determine connections among arteries, arterioles, and capillaries. Specifically, we sought to determine if capillaries of the SVP, ICP, and DCP had direct connections to arteries and arterioles. We also looked at patterns of vascular connections among the SVP, ICP, and DCP. We first identified a retinal artery, and its tributaries were traced manually at each branch point until the DCP was reached. Traced vessels were subsequently assigned orders using the Horton–Strahler nomenclature (Fig. 4). In brief, the Horton–Strahler scheme starts at the capillary level and proceeds centripetally.[44] The order is increased if two segments of equal order join at a bifurcation. The aim of the Horton–Strahler nomenclature is to group vessels with similar characteristics into one order. In this study, first-order vessels were defined as capillaries of the DCP, designated as ***c***. We also studied outflow patterns to determine connections among capillaries, venules, and veins. We studied how each individual plexus drained and communicated with a large venule. We also investigated whether venules from each plexus drained directly and independently into a vein located in the SVP or merged with draining venules from other plexuses prior to this. The Horton–Strahler nomenclature was again utilized to study draining patterns. Specifically, a DCP capillary loop (Fig. 4C) was first identified. The venules were manually traced until a v4 segment was reached. Retinal arteries and veins located in the plane of the SVP and within the boundaries of parafovea were designated as a4 and v4, respectively. Identifiable draining patterns of v3 into v4 were recorded for all 32 captured *z*-stacks. All vessel connection analyses, arterial inflow, and venous outflow pathways were traced by a single observer.

Vessel Diameter Measurements and Statistical Analysis

Vessel luminal diameters were recorded for all traced pathways from each confocal stack. Diameter was measured as the perpendicular distance across the maximum chord axis of each vessel. As lectin labels for the luminal endothelium, the entire labeled vessel was measured. In F-actin-labeled specimens, the endothelium, basement membrane, and smooth muscle cells (arterioles) were identifiable; only the luminal diameter was measured (Supplementary Fig. S1). Branching locations and sites of endothelial cell nuclei were avoided for diameter measurements. Arterioles and venules were often involved in multiple traced pathways; these vessels had their diameters recorded only once.

Data was analyzed using R (R Foundation for Statistical Computing, Vienna, Austria). The associations among

Investigative Ophthalmology & Visual Science

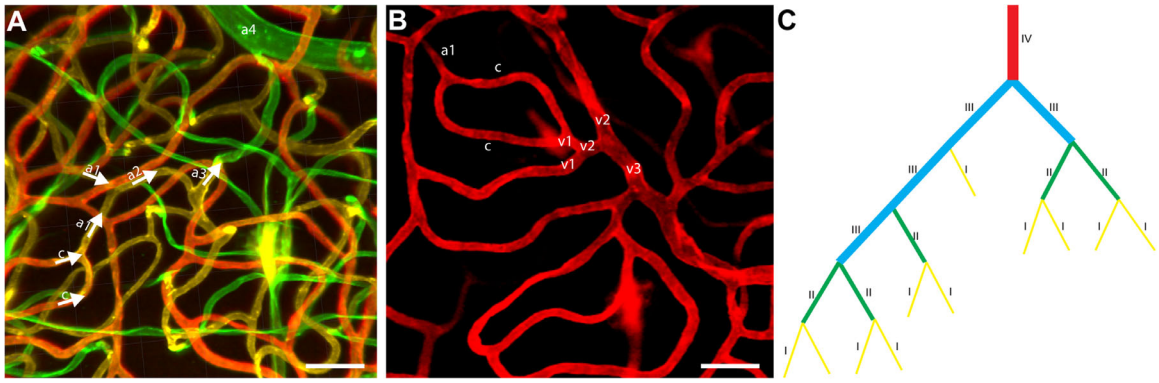

Figure 4. Classifying vascular order using the Horton–Strahler system. (**A**) Full-thickness, color-coded confocal stack encompassing all vascular plexuses illustrates the order of vessels in the arterial aspect of the microvasculature. The SVP is false-colored *green*, ICP is false-colored *yellow*, and DCP is false-colored *red*. Artery a4 is located in the SVP, and the capillary of interest (*c*) is located in the DCP. (**B**) Image of the DCP illustrating capillary loops and the orders of venules. (**C**) Schematic diagram of the Horton–Strahler order system illustrates the concept where a higher order vessel is formed by two similar sized tributary vessels. Confocal images in **A** and **B** were obtained from donor eye 12. *Scale bar*: 50 µm.

vessel diameter and vessel orders, age, and sex were determined using a multivariate linear mixed model. The random effects were left or right eye nested within donor identity to address the effects of both intra- and inter-eye correlations (where both eyes from a single donor were included). $P \leq 0.050$ was considered significant. Results were expressed as mean ± standard deviation.

Results

General

A total of 22 eyes were perfused and examined. Six eyes were excluded from the study due to incomplete labeling of the retinal vasculature secondary to postmortem vascular occlusions. The remaining 16 eyes with no history of eye disease were analyzed, including eight eyes from five female donors and eight eyes from seven male donors. The age range of donors was 18 to 89 years, with a mean age of 66.8 ± 21.9 years. Mean death-to-perfusion time was 5.2 ± 2.5 hours. Detailed donor demographic data and labeling performed for each eye can be found in the Table.

Table. Donor Information and Details Regarding Antibody Labeling Protocols

Eye	Age (y)	Sex	Cause of Death	Labeling Protocol
1	72	F	Endometrial Ca	αSMA/lectin
2	72	F	Endometrial Ca	αSMA/lectin
3	46	M	Angiosarcoma	αSMA/phalloidin
4	46	M	Angiosarcoma	αSMA/phalloidin
5	18	M	Drug overdose	αSMA/phalloidin
6	82	M	Ischemic CVA	αSMA/phalloidin
7	55	F	Renal cell Ca	Lectin
8	84	M	Ischemic CVA	Lectin
9	89	F	Hemorrhagic CVA	Lectin
10	89	F	Hemorrhagic CVA	Lectin
11	82	M	Ischemic CVA	Lectin
12	75	F	Endometrial Ca	Lectin
13	75	F	Endometrial Ca	Lectin
14	86	F	Lung Ca	Lectin
15	70	M	Sepsis	Lectin
16	42	M	Hemorrhagic CVA	Phalloidin

Eyes 1 and 2; 3 and 4; 9 and 10; and 12 and 13 were left and right eyes from the same donor. Ca, carcinoma; CVA, cerebrovascular accident.

Morphologic and Immunohistochemical Characteristics of the Retinal Circulation

Retinal arteries and veins were always found at the level of the SVP. Infrequently, both arteries and veins were seen to extend to the level of the ICP. Retinal arteries and veins were not seen at the level of the DCP. The morphology of the SVP, ICP, and DCP observed in this study was similar to what has been previously described[7] and is illustrated in Figure 5. Capillaries of the SVP demonstrated a predominantly 3D arrangement with numerous vertical connections to the ICP (Fig. 2). Capillaries of the ICP demonstrated greater tortuosity than other plexuses, as well as irregularly shaped capillary loops. Capillaries of the DCP were highly planar and one dimensional in configurations with multiple closed loops. Figure 6 illustrates the distribution of F-actin and αSMA in arteries, arterioles, and capillaries. All orders of vasculature demonstrated positive staining for F-actin. αSMA showed intense labeling in the smooth muscle cells and pericytes in the walls of arteries and arterioles. At the branch point of small arterioles within the ICP, colocalization of αSMA and nuclei revealed dome-shaped structures on the outer aspects of the vessel wall, consistent with previous descriptions of pericyte shape and location.[26,45,46] Such dome-shaped structures were also seen on the outer aspect of some capillaries in the SVP and ICP; however, they were not seen in the DCP. Capillary endothelia of the SVP and ICP demonstrated strong staining of αSMA, but only faint staining was seen in the endothelia of the DCP. The a1 vessels adjoining the ICP to the DCP demonstrated strong staining of αSMA proximally but there was an abrupt reduction in the intensity of staining within a1 vessels before connection to capillaries of the DCP (Fig. 6, inset I). Figure 7 illustrates the staining patterns of veins, venules, and capillaries with F-actin and αSMA. Weak staining of αSMA was seen within veins and venules. Unlike the arterial aspect, venous aspect capillaries of the SVP and ICP demonstrated

Investigative Ophthalmology & Visual Science

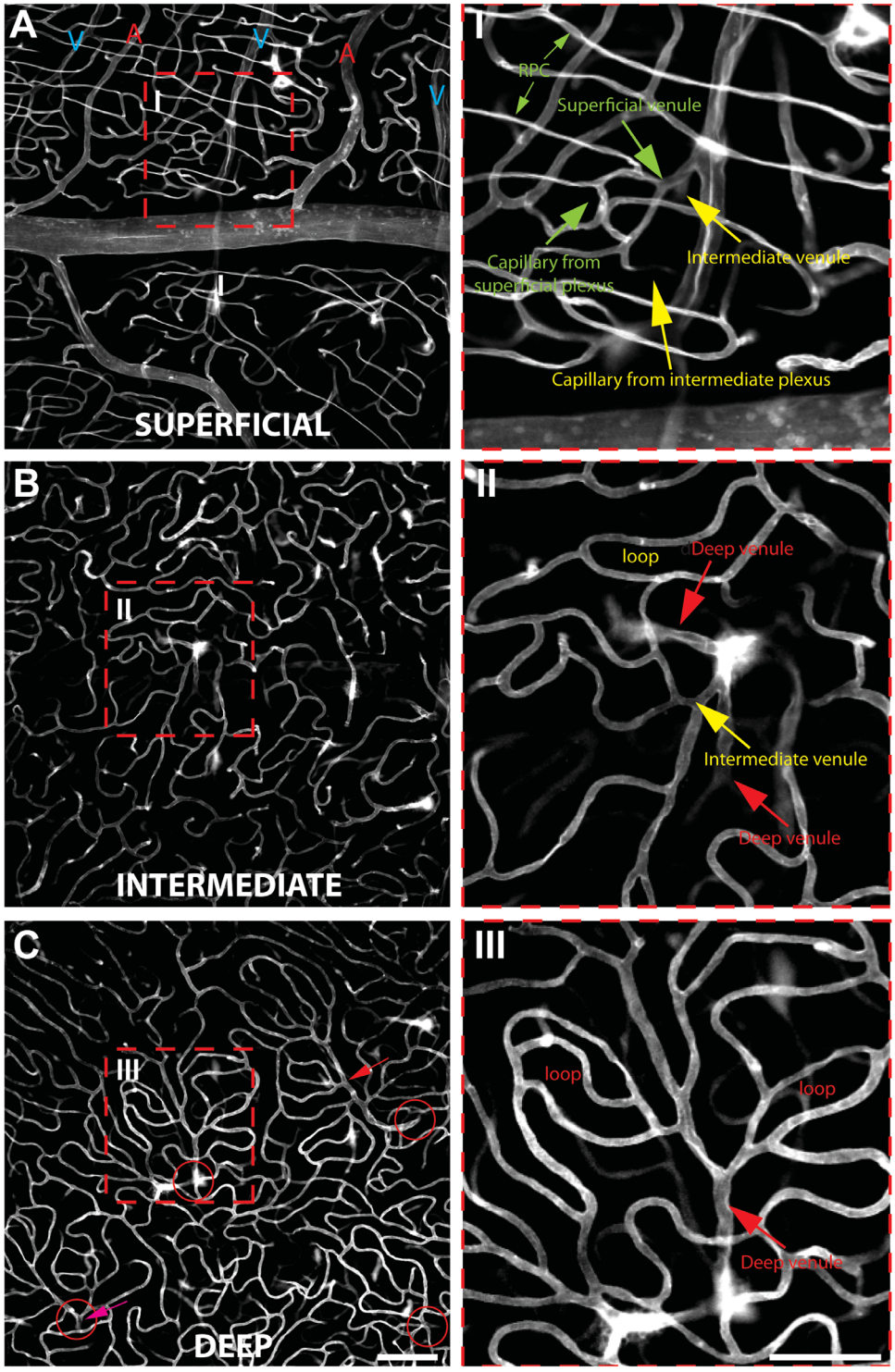

Figure 5. A lectin-labeled single confocal image stack, stratified into the (**A**) SVP, (**B**) ICP, and (**C**) DCP illustrating venular and capillary morphology, obtained from the superior parafovea of donor eye 12 (right eye). Retinal arteries (*A*) and veins (*V*) form interdigitating patterns in the SVP (**A**). SVP venules are usually short and numerous. Venules originating from ICP/DCP frequently join SVP venules prior to draining into a vein (inset I). SVP venules are responsible for draining capillaries of the SVP. When present along the arcades, retinal peripapillary capillaries (RPCs) also drain into the SVP venules (inset I). Capillaries of the ICP are tortuous, and few enclosed capillary loops can be identified (**B**). Venules of the ICP are often joined by venules of the DCP prior to draining into a vein (inset II). The ICP forms numerous connections with the SVP and DCP, evidenced by disjointed vessel segments identified in the en face plane (inset II). The DCP has a planar configuration with numerous enclosed capillary loops (**C**, inset III). In **C**, sites where v3 venules leave DCP and traverse superficially are marked with *red circles*. A vortex-like arrangement can be seen as adjacent capillaries and small venules drain toward these large venules. The v3 may have a long course within the DCP prior to ascending into the SVP (**C**, *red arrow*) or, shortly upon its formation, may ascend almost vertically into the SVP (**C**, *magenta arrow*). *Scale bars*: 60 µm.

Investigative Ophthalmology & Visual Science

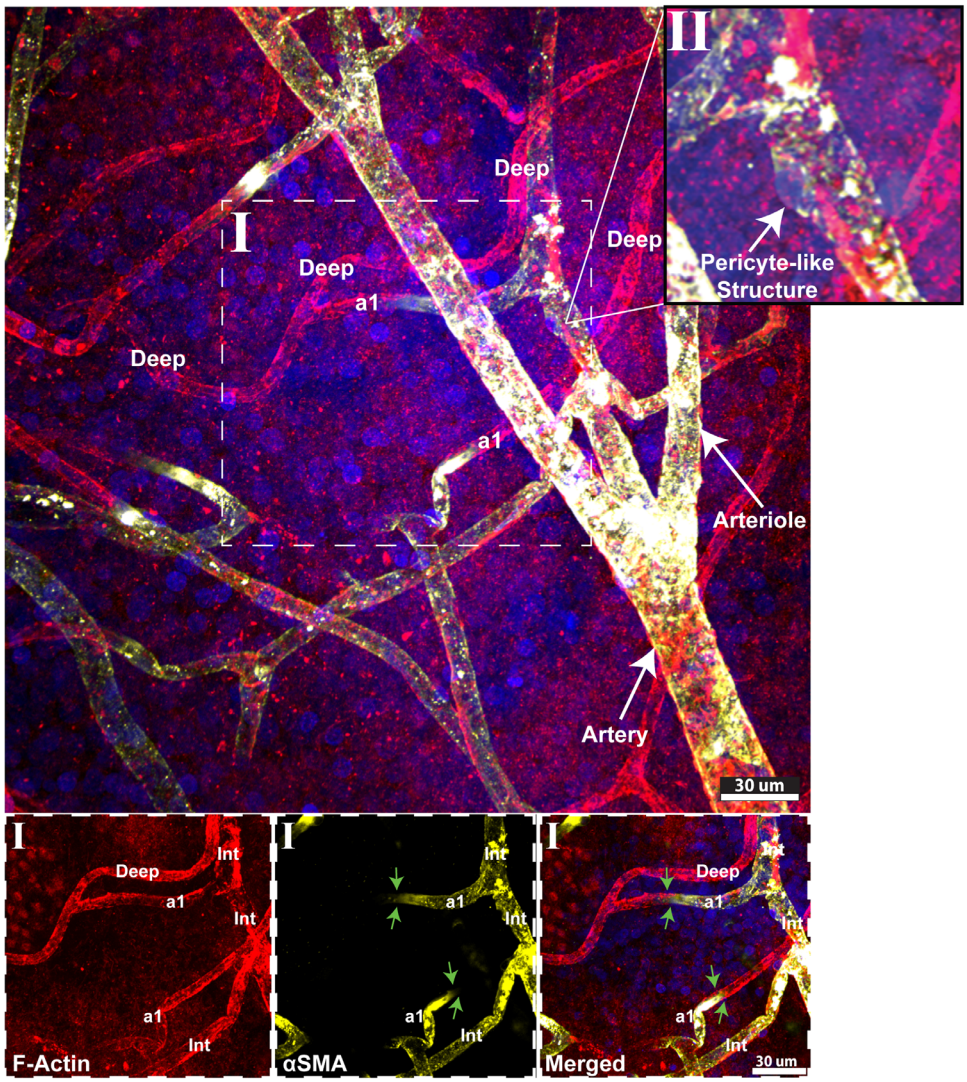

Figure 6. Staining patterns of arteries, arterioles and capillaries with F-actin and αSMA from donor eye 3. All orders of vasculature stained positive for F-actin. Arterioles and arteries stained intensely for αSMA. Capillaries on the arteriolar aspect showed moderate staining in the SVP and ICP. Inset I illustrate the variation in staining pattern of αSMA between the DCP and overlying capillary plexuses. Separate images for F-actin, αSMA, and merged channels are presented. Note that a1 segments, which are small arterioles that connect the ICP to the DCP, consistently demonstrate an abrupt reduction in intensity along their trajectory between the ICP and DCP (*green arrows*). Dome-shaped structures that resemble pericytes were identified as αSMA positive, external to vessel walls of small arterioles and capillaries, as highlighted in inset II. These structures were not identified in the DCP. *Red*, F-actin; *yellow*, αSMA; *blue*, nuclei.

weak staining of αSMA that was comparable to veins and venules. Strong staining of αSMA was also seen within a1 vessels and also at sites where venules connected to retinal veins. En face visualization at a lower magnification revealed abrupt termination of αSMA staining along the trajectory of capillaries between the arterial and venous aspects of the retinal circulation (Fig. 8). There was observably more αSMA stain within capillaries at the arterial aspect of the SVP and ICP compared to the venous aspect, as shown in Figure 8.

Inflow Analysis

In total, 150 inflow pathways were manually traced from all 16 eyes, and the different arterial inflow patterns are illustrated in Figure 9. On average, 11 outflow pathways were identified per 1 mm^2 of retina. Two different patterns were identified:

- Pattern 1 (79% of cases)—A retinal artery gave rise to an a3 arteriole at the level of the SVP that consequently communicated with the capillaries of the SVP. Smaller arterioles and capillaries of the SVP subsequently communicated with the ICP. Some a1 branches of these arterioles descended further to supply capillaries of the DCP.
- Pattern 2 (21% of cases)—A retinal artery gave rise to an a3 arteriole that traversed to the level of the ICP without any intermediary branches to the SVP. At the level of the ICP, the a3 arteriole and its branches supplied the capillaries of the ICP. As with Pattern 1, a1 branches originated from the ICP to supply capillaries of the DCP.

Investigative Ophthalmology & Visual Science

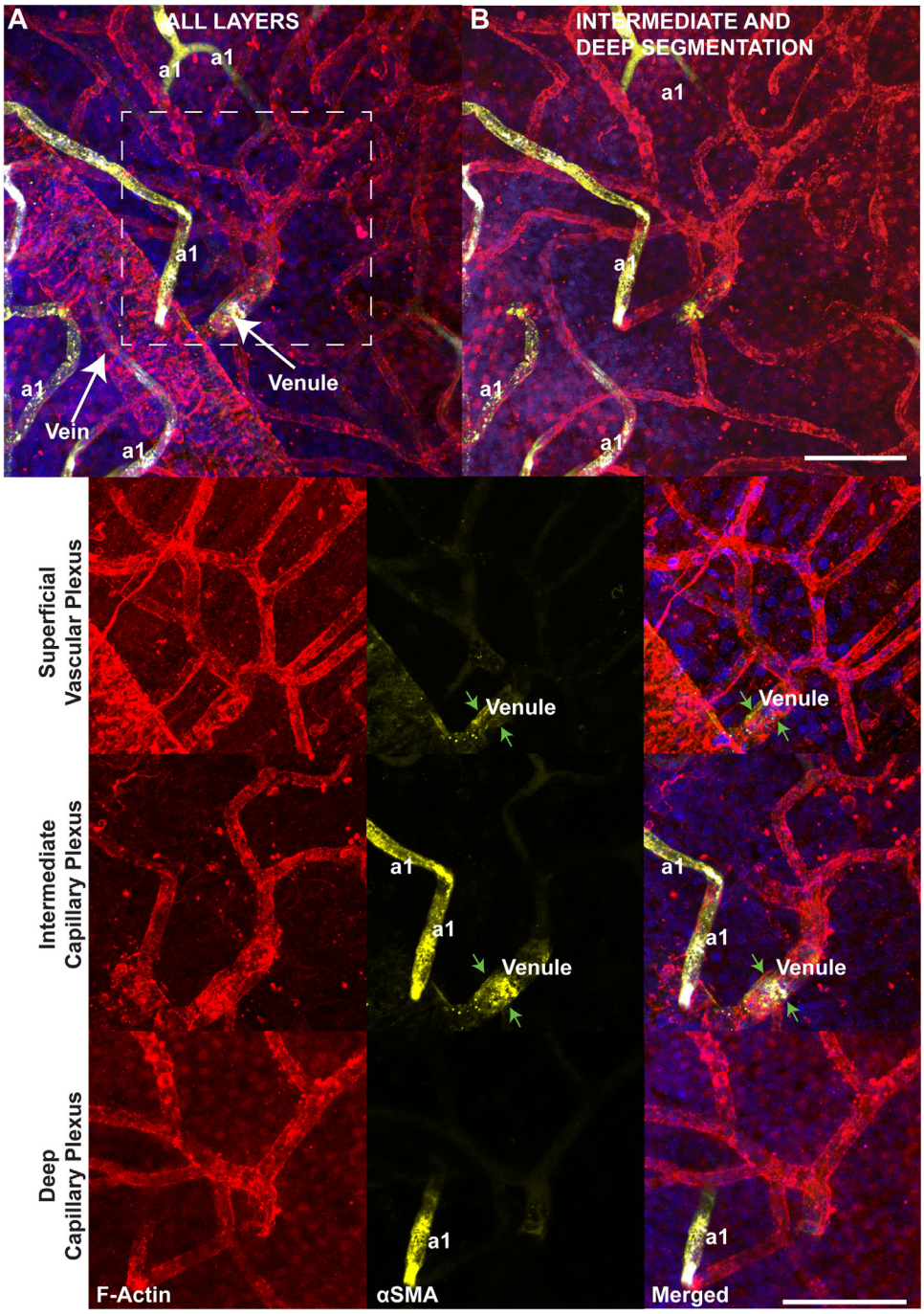

Figure 7. Staining patterns of veins, venules, and capillaries with F-actin and αSMA. (**A**) Diffuse F-actin staining is evident in all vessels. Veins and venules demonstrate weak staining of αSMA, as seen in a projected confocal stack that is comprised of all capillary plexuses. (**B**) Segmentation of the confocal stack to depict the combined ICP and DCP reveals that the staining intensity is high within a1 arterioles that connect the ICP to the DCP. Insets provide a stratified view of the SVP, ICP, and DCP. Separate images for F-actin, αSMA, and merged channels are presented. Note that there is only weak staining of capillaries with αSMA. In addition to a1 arterioles, there is also increased staining for αSMA at sites where venules connect to veins (*green arrows*). *Red*, F-actin; *yellow*, αSMA; *blue*, nuclei. *Scale bar*: 50 µm.

We did not find any examples of retinal arteries communicating directly and solely with capillaries of the DCP via descending arterioles. The origin of vascular inflow for the DCP was always the ICP, and this occurred in the form of a1 segments connecting the arterioles of the ICP to the DCP. At the level of the DCP, distal a1 was identified as the largest arteriole present. An a2 arteriole was not identified. When confocal volumes were rotated and viewed at different angles, there were observably more connections between the SVP and ICP than the ICP and DCP (Fig. 2A).

We also observed many instances where capillaries of the SVP communicated directly between retinal artery and retinal vein without forming any communications with capillaries of the ICP. Supplementary Figure S2 presents an en

Investigative Ophthalmology & Visual Science

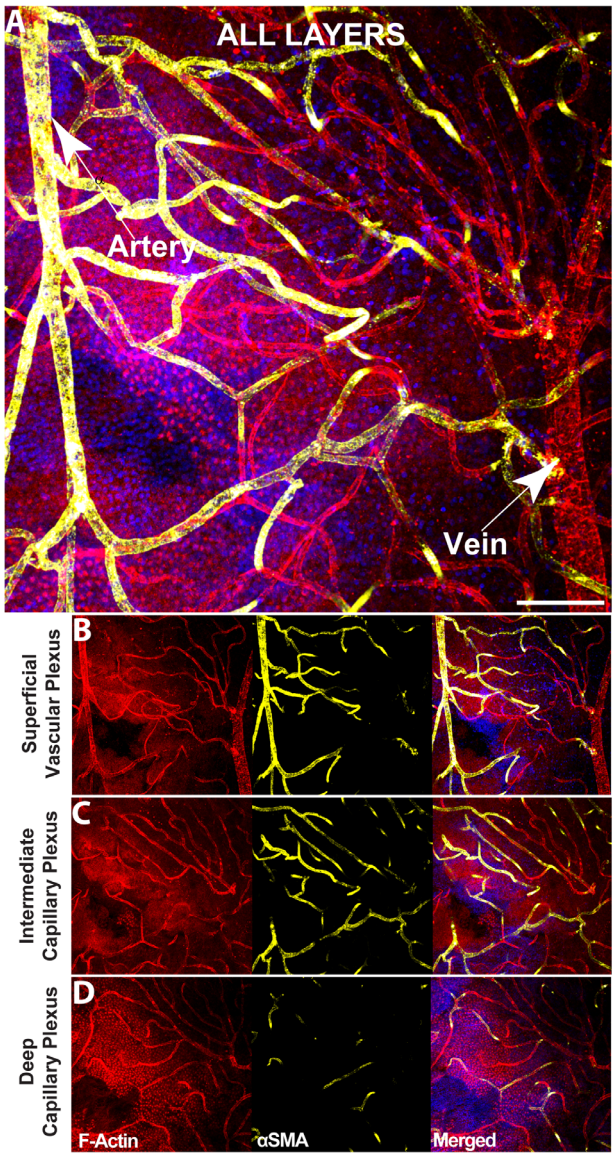

Figure 8. Topographic patterns of αSMA staining within the parafoveal circulation and variations in staining relative to retinal depth. An en face view of a projected confocal stack comprised of all capillary plexuses (**A**) reveals an observable variation in αSMA staining between the arterial and venous portions of the parafoveal circulation. Note that the intensity of αSMA staining is observably greater at the arterial side of the circulation. Stratified views of the SVP (**B**), ICP (**C**), and DCP (**D**) are presented in the lower image panels. Separate images for F-actin, αSMA, and merged channels are displayed. Note that the increased pattern of αSMA staining in the arterial aspect of the circulation is maintained in the SVP and ICP. The DCP is largely devoid of αSMA staining. Collectively, these findings illustrate a variation in αSMA distribution in the *x*, *y*, and *z* planes. *Red*, F-actin; *yellow*, αSMA; *blue*, nuclei. *Scale bar*: 50 µm.

face and transverse slab of the SVP that has been segmented between the inner limiting membrane and the outer border of retinal ganglion cell layer. Note that capillaries overlying the plane of the retinal GCL can be seen to run between the retinal artery and vein without descending below the plane of the RGC layer.

Outflow Analysis

We identified 150 venous outflow pathways from all 16 eyes. On average, 11 outflow pathways were identified per 1 mm^2 of retina. The different venous outflow patterns identified in this study are illustrated in Figure 10. Seven different outflow patterns were identified as follows:

- Pattern 1 (34.2%)—v3 of the SVP drains directly into the retinal vein (v4).
- Pattern 2 (7.6%)—v3 of the ICP drains directly into v4.
- Pattern 3 (4.0%)—v3 of the DCP drains directly into v4.
- Pattern 4 (18.9%)—Convergence of v3 from ICP and SVP prior to drainage into v4.
- Pattern 5 (1.7%)—Convergence of v3 from DCP and SVP prior to drainage into a v4.
- Pattern 6 (15.6%)—Convergence of v3 from the DCP and ICP prior to drainage into v4.
- Pattern 7 (17.9%)—Convergence of v3 from DCP, ICP, and SVP prior to drainage into v4.

Venules were identified retrogradely by first identifying a large vein (v4) within the SVP based on the definitions discussed previously and then traced along the venules until a DCP/ICP capillary loop was reached. We found that each of the capillary plexuses drained into v3 within the plexus. The v3 subsequently drained into v4 located at the plane of the SVP either directly or converged with one or more v3 from other plexuses prior to draining into v4. Across all sampling regions, we found 219 examples of v3 at the level of the SVP, 181 examples of v3 at the level of the ICP, and 118 examples of v3 at the level of the DCP. When viewed in the en face plane, the morphology of the venules at the levels of the DCP, ICP, and SVP differed (Fig. 5). The SVP vasculature has a distinct interdigitating arrangement of small arteries and veins; v3 of the SVP are typically short and numerous and drain capillaries of the SVP and RPC (when present). Some capillaries of the ICP were also seen to traverse superficially and drain via the SVP venules, as illustrated in Figure 5B. The ICP has highly irregular structures that include complete and incomplete capillary loops and numerous tortuous connecting vessels (Fig. 5C); v3 of the ICP are usually short and positioned in close proximity to a vein. They frequently drain into a v4 in conjunction with v3 of the SVP or DCP, or both. The DCP has a laminar arrangement with numerous capillary loops converging, eventually forming a central draining v3, giving a "vortex" like appearance[21] (Fig. 5C). The v3 were found to have highly variable lengths within the DCP prior to draining into the SVP. The v3 arising within locations distant from a retinal vein have a long course within the DCP and traverse superiorly in an oblique fashion. The v3 that arise from DCP adjacent to or directly underneath a retinal vein have a short and vertical course. In comparison, v3 of the SCP and ICP were generally short and formed by merging v2 segments adjacent to a retinal vein."

Vessel Diameter Analysis

The diameters and comparisons of the different orders of the retinal circulation are illustrated in Figure 11. With respect to vessel orders, v1 (9.8 ± 0.9 µm) and v4 (36.7 ± 6.1 µm) had significantly larger diameter than their counterparts a1 (8.4 ± 0.8 µm; $P = 0.025$) and a4 (31.5 ± 7.6 µm; $P < 0.001$). The segments of a2/v2 (10.9 ± 1.6 µm vs. 12.1 ± 1.4 µm;

Investigative Ophthalmology & Visual Science

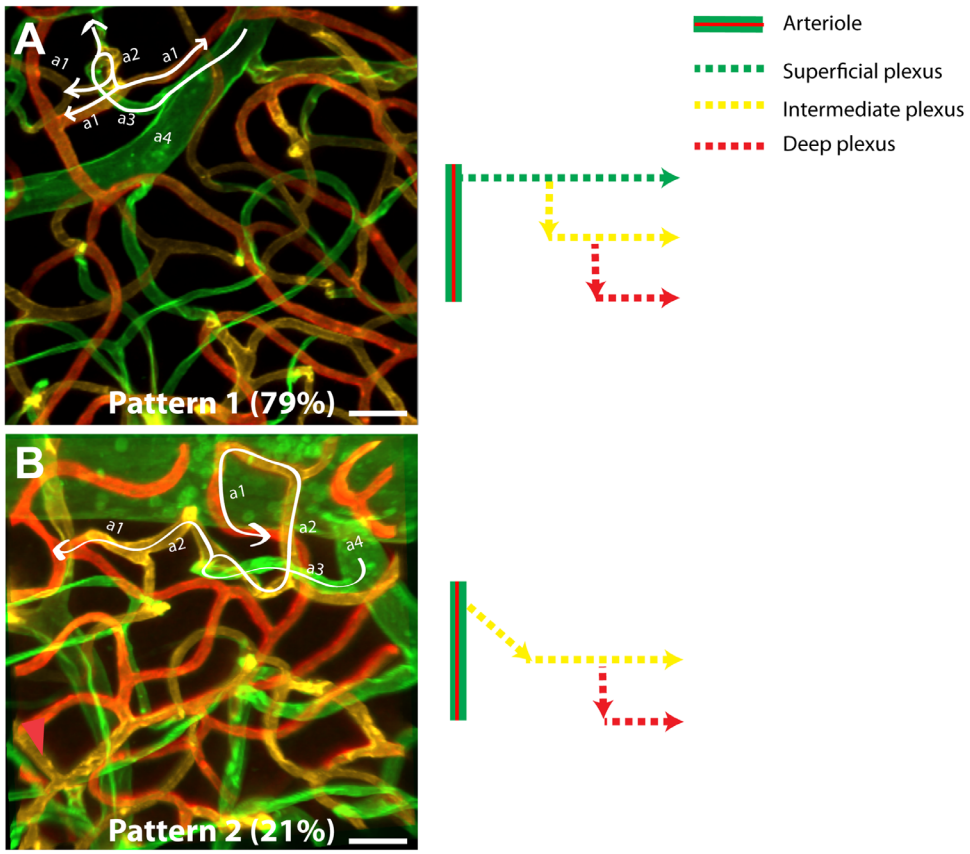

Figure 9. Arterial inflow patterns in the parafovea. Two different patterns of arterial inflow were identified. (**A**) Pattern 1 (79%) was characterized by the ICP being supplied by an arteriole originating from the SVP. Arteriole branches from the ICP subsequently supplied the DCP. (**B**) The remaining 21% of inflow pathways were Pattern 2, where the artery directly gave rise to an arteriole that supplies the ICP without supplying the SVP. Branches originating from the ICP subsequently supplied the DCP. There were no cases where an artery or arteriole at the level of the SVP directly supplied the DCP, bypassing the ICP. Manual tracings of the inflow patterns are provided on the *z*-projected confocal images that have been false-colored *green* (SVP), *yellow* (ICP), and *red* (DCP). A schematic illustration of each pattern is also provided. *Scale bar*: 50 µm.

$P = 0.084$) and a3/v3 (17.9 ± 4.2 µm vs. 18.8 ± 4.0 µm; $P = 0.244$) were not significantly different. In addition, both a1 and v1 were significantly larger than DCP capillaries (6.9 ± 0.9 µm; both $P < 0.001$). Mean capillary diameter was increased by 0.04 µm for every year of age ($P = 0.048$). There was no difference in diameter between males and females ($P = 0.529$).

Discussion

The seminal work by Zweifach[24] in 1937 showed that reliable categorization of the different segments of the microvasculature requires integration of data concerning vascular diameter, density, and organization of perivascular elements and the relationship of the vessels to the vascular system as a whole. These findings were reaffirmed by the subsequent ultrastructural studies of the mammalian arterial and venous systems by Rhodin.[42,47] The importance of considering other properties of the vascular system, aside from luminal diameter, is that these additional criteria convey vital information regarding the rheologic and hemodynamic properties of the regional microcirculation. They also convey critical information about regional mechanisms that control blood flow and, by extension, the vulnerability of distinct capillary plexuses to ischemic injury. This report has focused only on the microvasculature of human parafovea due to our limited understanding of its complex structures and its importance in understanding the pathogenesis of many sight-threatening diseases. We have differentiated the parafoveal circulation into arterial, arteriole, capillary, venule, and venous segments by incorporating data concerning luminal diameter, perivascular smooth muscle cell organization, and endothelial morphology and loop structures. These histologic parameters have been validated in previous studies[4,39,40,48,49] and are used hitherto to propose a three-dimensional model of the normal parafoveal human circulation (Fig. 12).

Consistent with previous histologic studies,[7–10,28] we determined that the parafoveal circulation is comprised of three capillary plexuses; however, we found that not all were directly supplied by a retinal arteriole originating from a retinal artery. In this report, an arteriole was defined as a vascular structure between 8 and 15 µm in diameter.[40] An arteriole was differentiated from a venule by its thicker wall and a circular pattern of smooth muscle cells (usually one layer) encircling it.[40] Arterioles defined per our criteria were seen at the level of the SVP and ICP. We found clear examples of arterioles connecting to retinal arteries and the capillary beds of the SVP and ICP. The most common pattern of arterial inflow was an arteriole that fed the capillary beds of the

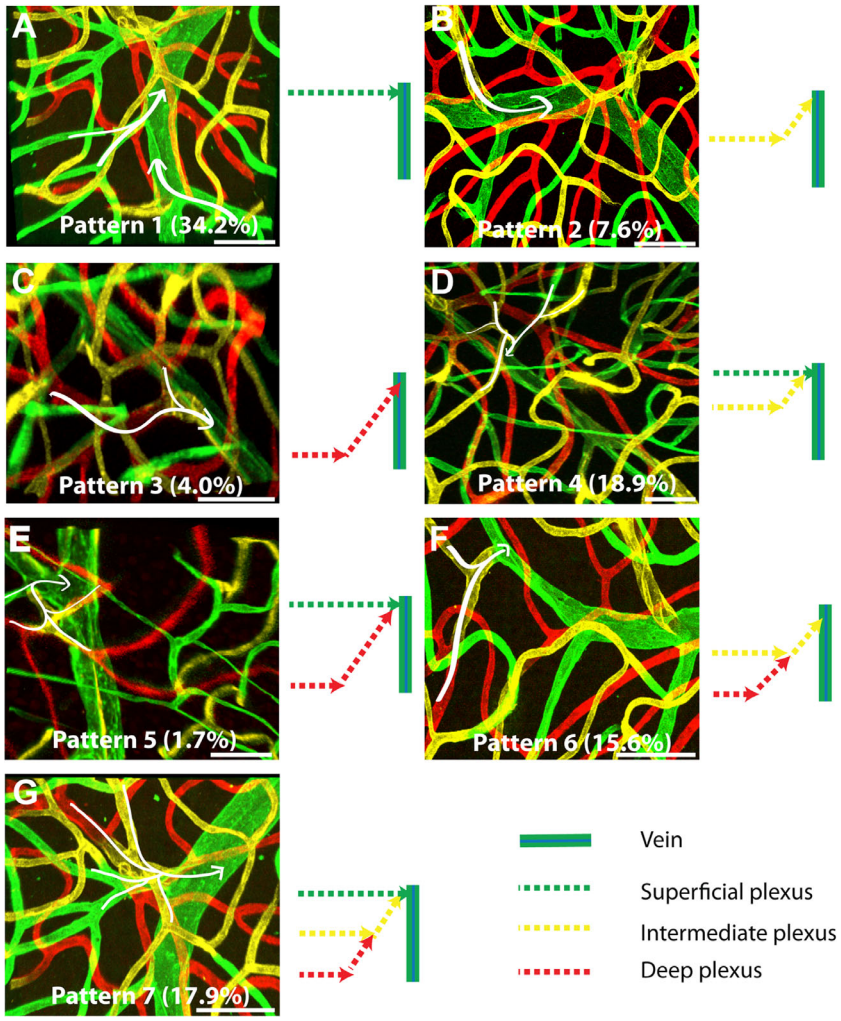

Figure 10. Venous outflow patterns in the parafovea. A total of seven different patterns were identified. Patterns 1 to 3 illustrate examples of the (**A**) SVP, (**B**) ICP, and (**C**) DCP, which form venules that independently drain into a vein (v4) at the level of the SVP. (**D–F**) Patterns 4 to 6 illustrate examples where venules from two plexuses converge and drain into a v4. (**G**) Pattern 7 illustrates an example of when all three plexuses draining venules converge and drain into a v4. Images were rotated in 3D for illustration purpose and are not to the same scale. The *z*-axis of each image was elongated by a factor of 2.5 to facilitate visualization of planes. Manual tracings of the outflow patterns are provided on the confocal images that have been false-colored *green* (SVP), *yellow* (ICP), and *red* (DCP). Schematic illustrations and frequency of each pattern are also provided. *Scale bars*: 60 µm.

SVP before diving to the level of the ICP to feed capillaries in this plane. Less frequently (21% of instances), arterioles were found to arise from retinal arteries and descend to the level of the ICP without any tributary branches to the SVP. We did not find any examples of an arteriole that formed a direct connection between capillaries of the DCP and a retinal artery. Instead, small arterioles that supply the DCP (a1) always originated from arterioles of the ICP. Taken together, our findings suggest that blood flow in the DCP may be intricately dependent upon and regulated by the ICP. Our findings also implicate a series and parallel arrangement of parafoveal arterial inflow pathways that is similar to what has been previously reported in the peripapillary region.[50]

Our study demonstrates significant asymmetry between arterial inflow and venous outflow pathways in the human parafovea. Retinal veins were found at the level of the SVP, and we identified a total of seven different outflow pathways connecting the capillary plexuses to the retinal vein. We identified v3-order venules at the level of the SVP, ICP, and DCP. In contrast to the lack of direct arteriolar supply to the DCP, we found examples of venules at the level of the DCP draining directly into the retinal vein without communicating with outflow channels at the level of the SVP and ICP. In this regard, our study supports the previous finding by Snodderly and Weinhaus [9] that showed that the geometry of the venous drainage system in the squirrel monkey was significantly different from the arterial inflow system. Similar to their report, we also found examples of biconvergence and triconvergence of venules of different plexuses prior to drainage into retinal veins.

The retinal circulation lacks autonomic innervation.[51–53] Rapid fluctuations in neuronal metabolic demands due to shifts from photopic and scotopic conditions are predominantly governed by autoregulation and local blood flow control mechanisms.[2] Smooth muscle cells and pericytes represent the principal myogenic mechanisms for retinal vascular autoregulation and are able to control blood flow by regulating vascular diameter and resistance.[2,54] Hogan

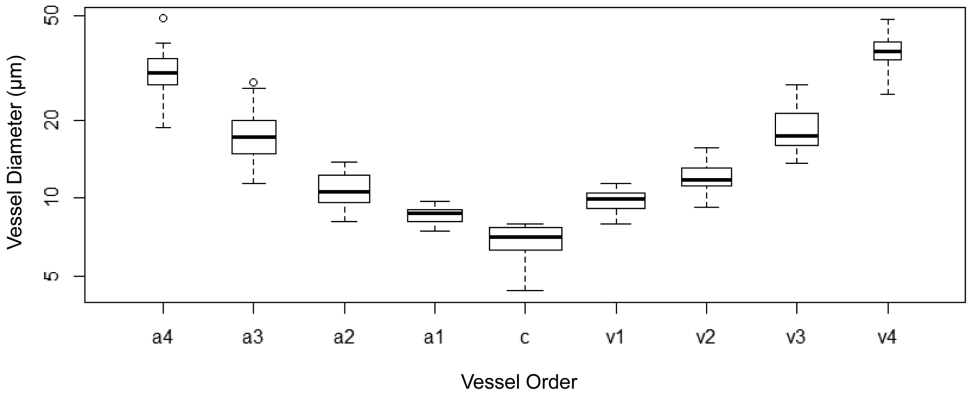

Figure 11. Vessel diameter was plotted for each order of vessel. The median, 25% to 75% interquartile range, and 95% interval are shown with each boxplot. Vessel diameter *y*-axis is presented in log scale to best illustrate the differences among a1, capillary, and v1. The terminal arteriole (a1), which supplies the DCP, had a mean diameter of 8.4 μm, significantly smaller than v1 (9.8 μm) and v3, the draining venule of the DCP (18.8 μm). Capillaries of the DCP had a mean diameter of 6.9 μm. a2/v2 and a3/v3 were comparable in size. v4 was found to be larger than a4 by a mean value of 5.2 μm. Capillary, $n = 228$; a1, $n = 165$; a2, $n = 128$; a3, $n = 98$; a4, $n = 40$; v1, $n = 169$; v2, $n = 120$; v3, $n = 77$; v4, $n = 32$. Width of each box reflects on the sample sizes with logscale.

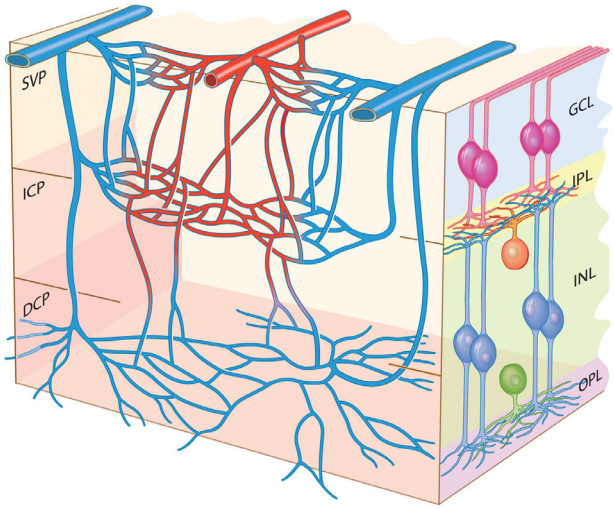

Figure 12. Schematic representation of the parafoveal circulation. The SVP is located at the level of the GCL. The ICP is located between the inner plexiform layer and the inner aspect of the inner nuclear layer (INL). The DCP is located within the outer aspect of the INL and outer plexiform layer. Both SVP and ICP receive direct arteriolar supply from a retinal artery. The SVP and ICP are interconnected by numerous vessels on both the arteriolar and venular aspects. In contrast, the DCP is supplied only by small arterioles that originate from the ICP. All three plexuses form venules that drain into the retinal vein located at the level of the SVP. A venule may drain directly into a vein or converge with venules from another plexus prior to draining into a vein.

and Feeney[39,40] found that smooth muscle cells envelop large arterioles, whereas pericytes surround smaller arterioles and capillaries that are less than 8 μm in diameter. They were found at sites of vascular bifurcation and were proposed to perform a sphincter-like function.[26] This observation is corroborated in the present report and has also been reported in the brain.[34] A major contractile protein expressed by pericytes and smooth muscle cells that mediates vasoregulation is αSMA.[26,55,56] The presence of cytoplasmic αSMA in pericytes and smooth muscle cells implicates some degree of overlapping function by these cells. In our recent study, we quantified αSMA labeling in the normal human macula and found that staining for this protein was greatest in arteries/arterioles less than 60 μm in diameter.[25] We also found that the magnitude of αSMA staining was not proportional to the amount of vascular smooth muscle cells or endothelium present.[57]

The present report is an extension of this previous study, as we sought to examine the profile of αSMA staining change among different capillary networks and also between the arterial and venous portions of the retinal circulation. In this study, we demonstrate an observable change in αSMA between arterial and venous portions of the retinal circulation. Capillary vessels closer to retinal arteries demonstrated increased staining in comparison to those capillaries in proximity to retinal veins; however, detection of the dome-shaped pericyte-like structures using αSMA may underestimate its density.[55] We found that pericytes were sparsely distributed, whereas Frank et al.,[58] in their electron microscopy study, found an almost 1:2 ratio of pericytes to endothelial cells. Previous animal studies[26,56,59] found that pericyte αSMA labeling intensity varied significantly among vascular plexuses, especially in the DCP, where they were frequently undetectable; therefore, one reason why pericytes were not clearly seen in the DCP in our study could be due to the staining protocol used. It is possible that a greater number of pericytes may have been detected in the DCP if a pericyte-specific antibody such as NG2 was used and/or combined with electron microscopy studies that allow precise visualization of cellular morphology. This important issue requires reconciliation with further studies.

Following the observation of collateral vessels in the deep retinal layers following RVO, Henkind and Wise[13] proposed that the deep circulation serves a predominantly venous function. Their observations, however, were not supported by the histologic studies by Michaelson and Campbell.[6] The variations in αSMA staining between upstream and downstream capillaries of the SVP and ICP suggest that these capillaries serve differing physiologic functions; that is, the ICP and SVP can be subdivided into arterial and venous portions. In other vascular beds of the human body, the frequency and amplitude of vasoconstriction mediated by αSMA in arterial and venous beds are different.[60] We did not evaluate the tonic versus phasic contractile properties

Investigative Ophthalmology & Visual Science

of αSMA in the parafovea but propose that this issue should be further studied, as it is likely to expand our understanding of the mechanisms that control retina blood flow.

Another important finding in this study is the observable increase in αSMA stain within a1 arterioles that connect the ICP to the DCP. This suggests that a1 may function as one of the vital control points for blood flow to the DCP. Although retinal veins were largely devoid of αSMA, we consistently found focal points of increased staining at sites where venules joined veins. Using isolated porcine preparations, we have previously shown that the tone of retinal veins can be modulated by tissue-generated vasoactive factors such as endothelin-1.[61] Increased staining at the point of a venule–vein junction may signify the presence of sphincter-like mechanisms. Therefore, in a similar manner by which major arterial inflow is controlled by smooth muscle cells and pericytes,[59] a control point for major venous outflow may also be present within the parafovea at the junction between venules and veins. The previous study involving rats by Kornfield and Newman[59] demonstrated that blood flow in the three capillary layers of the rodent retina is differentially regulated. In addition to larger arterioles, a1 arterioles and venule/vein junctions may also be important for maintaining this differential regulation.

The findings in this study may form the basis for understanding some of the pathogenic mechanisms underlying DR and RVO. Previous studies have shown that the DCP is preferentially altered in the early stages of DR.[62–65] Pericyte loss[66–68] and, by extension, loss of αSMA are also known to be hallmark features of early DR. As the DCP does not have direct communications to retinal arteries, its blood supply is dependent on the ICP and a1 arterioles. It is plausible that loss of pericytes surrounding a1 arterioles may limit blood flow to the DCP in hypoxic states such as DR. This issue may be compounded by the inherent lack of αSMA content and autoregulatory ability of the DCP. Histologic and OCTA studies have also shown that collateral vessels following branch RVO are preferentially found in the plane of the DCP.[13,69,70] One mechanism that may account for this manifestation is the relatively lower αSMA expression in vessels of the DCP. As such, these vessels may be inherently more distensible than vessels of the SVP and ICP that are more frequently surrounded by αSMA-expressing pericytes and smooth muscle cells.

The lack of arteriolar supply of the DCP may also play an important role in PAMM. In a study of more than 400 subjects with CRVO, Rahimy et al.[71] identified acute PAMM lesions in 5% of cases. These are hyperreflective lesions that originate from the INL/OPL junction; they can be observed using OCT and have been described as having a fern-like appearance with perivenular involvement.[72,73] The current understanding of the formation of PAMM is derived from the Krogh cylinder model,[74] which is based on perfusion of muscle tissue. It assumes that the microvasculature is comprised of independent capillary units, each consisting of a feeding arteriole, a capillary bed, and a draining venule. When applied to the macula circulation, the venule of the DCP is thought to act as the major venous outflow system, thus putting the DCP at the distal end of the oxygen supply chain, forming the hypoxic compartment.[75] However, based on our current model (Fig. 12), the parafoveal angioarchitecture differs from a Krogh cylinder in that we observed no distinct circulatory units. With a significantly elevated venous resistance, blood flow through the retinal vasculature is limited. As we have shown that all three plexuses possess v3-order venules that connect directly to the retinal vein system, resistance in each capillary plexus is expected to be elevated. For flow to occur, the perfusion pressure of the plexuses must overcome this resistance, and this is not likely to occur in the DCP, which lacks a large arteriolar supply, possibly leading to ischemia of the INL/OPL junction.

This report has a number of strengths. We utilized perfusion-based labeling of a relatively large number of human donor eyes to achieve complete retinal labeling. We also coupled high-resolution confocal microscopy with state-of-the-art image analysis software to quantify the connectivity of the parafoveal circulation in three dimensions. Finally, we used histologic structural criteria to segment the retinal vascular tree, which we propose has more relevance for inferring knowledge about regional hemodynamic properties than a construct that relies purely on vascular diameter. Collectively, this histologic information may be used to better interpret clinical imaging data such as OCTA. We acknowledge several limitations of this study: (1) Only the parafovea of the retina was studied; therefore, the findings of this study may not apply to other parts of the retina. (2) A single observer was utilized to trace the arterial and venous pathways. (3) Luminal diameter measurements did not take into consideration possible contribution from factors such as retinal stretch from refractive error, as such information was not available. (4) Pathogenic mechanisms regarding DR, RVO, and PAMM are speculative and will require further work for validation. (5) The important relationships among astrocytes, Müller cells, and each of the capillary plexuses were not evaluated.

Acknowledgments

The authors thank staff from the Lions Eye Bank of Western Australia, Lions Eye Institute, for provision of human donor eyes, and staff from DonateLife WA, the Western Australian agency for organ and tissue donation, who facilitated the recruitment of donors into the study by referral and completion of consent processes.

Grant support was provided by an Investigator Grant of the National Health and Medical Research Council of Australia (APP1173403).

Disclosure: **D. An,** None; **P. Yu,** None; **K.B. Freund,** Optovue (C), Heidelberg Engineering (C), Zeiss (C), Allergan (C), Bayer (C), Genentech/Roche (C, F), Novartis (C); **D.-Y. Yu,** None; **C. Balaratnasingam,** Novartis (C), Roche (C), Allergan (C), Bayer (C)

References

1. Yu D-Y, Cringle SJ. Oxygen distribution and consumption within the retina in vascularised and avascular retinas and in animal models of retinal disease. *Prog Retin Eye Res*. 2001;20:175–208.
2. Yu DY, Cringle SJ, Yu PK, et al. Retinal capillary perfusion: spatial and temporal heterogeneity. *Prog Retin Eye Res*. 2019;70:23–54.
3. Ames A. Energy requirements of CNS cells as related to their function and to their vulnerability to ischemia: a commentary based on studies on retina. *Can J Pharmacol*. 1992;70:S158–S164.
4. Yu DY, Yu PK, Cringle SJ, Kang MH, Su EN. Functional and morphological characteristics of the retinal and choroidal vasculature. *Prog Retin Eye Res*. 2014;40:53–93.

5. Hogan MJ, Alvarado JA, Weddell JE. *Histology of the Human Eye: An Atlas and Textbook*. Philadelphia, PA: W.B. Saunders Company; 1971.
6. Michaelson IC, Campbell ACP. The anatomy of the finer retinal vessels, and some observations on their significance in certain retinal diseases. *Trans Ophthalmol Soc UK*. 1940;60:71–111.
7. Chan G, Balaratnasingam C, Yu PK, et al. Quantitative morphometry of perifoveal capillary networks in the human retina. *Invest Ophthalmol Vis Sci*. 2012;53:5502–5514.
8. Balaratnasingam C, An D, Sakurada Y, et al. Comparisons between histology and optical coherence tomography angiography of the periarterial capillary-free zone. *Am J Ophthalmol*. 2018;189:55–64.
9. Snodderly DM, Weinhaus RS. Retinal vasculature of the fovea of the squirrel monkey, *Saimiri sciureus*: three-dimensional architecture, visual screening, and relationships to the neuronal layers. *J Compar Neurol*. 1990;297:145–163.
10. Snodderly DM, Weinhaus RS, Choi JC. Neural-vascular relationships in central retina of macaque monkeys (*Macaca fascicularis*). *J Neuroscience*. 1992;12:1169–1193.
11. Toussaint D, Kuwabara T, Cogan DG. Retinal vascular patterns. II. Human retinal vessels studied in three dimensions. *Arch Ophthalmol*. 1961;65:575–581.
12. Kuwabara T, Cogan DG. Studies of retinal vascular patterns. Part 1. Normal architecture. *Arch Ophthalmol*. 1960;64:904–911.
13. Henkind P, Wise GN. Retinal neovascularization, collaterals, and vascular shunts. *Br J Ophthalmol*. 1974;58:413–422.
14. Balaratnasingam C, An D, Freund KB, Francke A, Yu DY. Correlation between histologic and OCT angiography analysis of macular circulation. *Ophthalmology*. 2019;126:1588–1589.
15. Spaide RF, Fujimoto JG, Waheed NK. Image artifacts in optical coherence tomography angiography. *Retina*. 2015;35:2163–2180.
16. Corvi F, Cozzi M, Belotti M, Nizza D, Staurenghi G, Giani A. Comparison between several optical coherence tomography angiography devices and indocyanine green angiography of choroidal neovascularization. *Invest Ophthalmol Vis Sci*. 2019;60:4551.
17. Spaide RF, Fujimoto JG, Waheed NK, Sadda SR, Staurenghi G. Optical coherence tomography angiography. *Prog Retin Eye Res*. 2018;64:1–55.
18. Ma J, Desai R, Nesper P, Gill M, Fawzi A, Skondra D. Optical coherence tomographic angiography imaging in age-related macular degeneration. *Ophthalmol Eye Dis*. 2017;9:1179172116686075.
19. Jia Y, Tan O, Tokayer J, et al. Split-spectrum amplitude-decorrelation angiography with optical coherence tomography. *Opt Express*. 2012;20:4710–4725.
20. Nesper PL, Fawzi AA. Human parafoveal capillary vascular anatomy and connectivity revealed by optical coherence tomography angiography. *Invest Ophthalmol Vis Sci*. 2018;59:3858–3867.
21. Campbell JP, Zhang M, Hwang TS, et al. Detailed vascular anatomy of the human retina by projection-resolved optical coherence tomography angiography. *Sci Rep*. 2017;7:42201.
22. Bonnin S, Mane V, Couturier A, et al. New insight into the macular deep vascular plexus imaged by optical coherence tomography angiography. *Retina*. 2015;35:2347–2352.
23. Garrity ST, Paques M, Gaudric A, Freund KB, Sarraf D. Considerations in the understanding of venous outflow in the retinal capillary plexus. *Retina*. 2017;37:1809–1812.
24. Zweifach BW. The structure and reactions of the small blood vessels in Amphibia. *Am J Anat*. 1937;60:473–514.
25. Yu PK, An D, Balaratnasingam C, Cringle SJ, Yu DY. Topographic distribution of contractile protein in the human macular microvasculature. *Invest Ophthalmol Vis Sci*. 2019;60:4574–4582.
26. Nehls V, Drenckhahn D. Heterogeneity of microvascular pericytes for smooth muscle type alpha-actin. *J Cell Biol*. 1991;113:147–154.
27. Yu DY, Su EN, Cringle SJ, Yu PK. Isolated preparations of ocular vasculature and their applications in ophthalmic research. *Prog Retin Eye Res*. 2003;22:135–169.
28. Yu PK, Mammo Z, Balaratnasingam C, Yu DY. Quantitative study of the macular microvasculature in human donor eyes. *Invest Ophthalmol Vis Sci*. 2018;59:108–116.
29. An D, Balaratnasingam C, Heisler M, et al. Quantitative comparisons between optical coherence tomography angiography and matched histology in the human eye. *Exp Eye Res*. 2018;170:13–19.
30. Yu DY, Yu PK, Balaratnasingam C, Cringle SJ, Su EN. Microscopic structure of the retina and vasculature in the human eye. In: Méndez-Vilas A, Díaz J , eds. *Microscopy: Science, Technology, Applications and Education*. Badajoz, Spain: Formatex Research Center; 2010:867–875.
31. Toribatake Y, Tomita K, Kawahara N, Baba H, Ohnari H, Tanaka S. Regulation of vasomotion of arterioles and capillaries in the cat spinal cord: role of alpha actin and endothelin-1. *Spinal Cord*. 1997;35:26–32.
32. Skalli O, Pelte MF, Peclet MC, et al. Alpha-smooth muscle actin, a differentiation marker of smooth muscle cells, is present in microfilamentous bundles of pericytes. *J Histochem Cytochem*. 1989;37:315–321.
33. Shepro D, Morel NML. Pericyte physiology. *FASEB J*. 1993;7:1031–1038.
34. Reina-De La Torre F, Rodriguez-Baeza A, Sahuquillo-Barris J. Morphological characteristics and distribution pattern of the arterial vessels in human cerebral cortex: a scanning electron microscope study. *Anat Rec*. 1998;251:87–96.
35. Tan PE, Yu PK, Balaratnasingam C, et al. Quantitative confocal imaging of the retinal microvasculature in the human retina. *Invest Ophthalmol Vis Sci*. 2012;53:5728–5736.
36. Chan G, Balaratnasingam C, Yu PK, et al. Quantitative changes in perifoveal capillary networks in patients with vascular comorbidities. *Invest Ophthalmol Vis Sci*. 2013;54:5175–5185.
37. Yu PK. *Intracellular Structure and Function of Microvascular Endothelium in the Normal and Diabetic Eyes [thesis]*. Perth, Australia: The University of Western Australia; 2000.
38. Yu PK, Balaratnasingam C, Cringle SJ, McAllister IL, Provis J, Yu DY. Microstructure and network organization of the microvasculature in the human macula. *Invest Ophthalmol Vis Sci*. 2010;51:6735–6743.
39. Hogan MJ, Feeney L. The ultrastructure of the retinal blood vessels. I. The large vessels. *J Ultrastruct Res*. 1963;39:10–28.
40. Hogan MJ, Feeney L. The ultrastructure of the retinal vessels. II. The small vessels. *J Ultrastruct Res*. 1963;49:29–46.
41. Richard E, van Gool WA, Hoozemans JJ, et al. Morphometric changes in the cortical microvascular network in Alzheimer's disease. *J Alzheimers Dis*. 2010;22:811–818.
42. Rhodin JA. Ultrastructure of mammalian venous capillaries, venules, and small collecting veins. *J Ultrastruct Res*. 1968;25:452–500.
43. Yu PK, Balaratnasingam C, Morgan WH, Cringle SJ, McAllister IL, Yu DY. The structural relationship between the microvasculature, neurons, and glia in the human retina. *Invest Ophthalmol Vis Sci*. 2010;51:447–458.

Investigative Ophthalmology & Visual Science

44. Tuma RF, Duran WN, Ley K , eds. *Handbook of Physiology: Microcirculation*, 2nd ed. San Diego, CA: Academic Press; 2008.
45. Hirschi KK, D'Amore PA. Pericytes in the microvasculature. *Cardiovasc Res*. 1996;32:687–698.
46. Kuwabara T, Cogan DG. Retinal vascular patterns. VI. Mural cells of the retinal capillaries. *Arch Ophthalmol*. 1963;69:492–502.
47. Rhodin JA. The ultrastructure of mammalian arterioles and precapillary sphincters. *J Ultrastruct Res*. 1967;18:181–223.
48. Braverman IM, Yen A. Ultrastructure of the human dermal microcirculation. II. The capillary loops of the dermal papillae. *J Invest Dermatol*. 1977;68:44–52.
49. Factor SM, Okun EM, Minase T, Kirk ES. The microcirculation of the human heart: end-capillary loops with discrete perfusion fields. *Circulation*. 1982;66:1241–1248.
50. Chandrasekera E, An D, McAllister IL, Yu DY, Balaratnasingam C. Three-dimensional microscopy demonstrates series and parallel organization of human peripapillary capillary plexuses. *Invest Ophthalmol Vis Sci*. 2018;59:4327–4344.
51. Laties AM. Central retinal artery innervation. *Arch Ophthalmol*. 1967;77:405–409.
52. Ye X, Laties AM, Stone RA. Peptidergic innervation of the retinal vasculature and optic nerve head. *Invest Ophthalmol Vis Sci*. 1990;31:1731–1737.
53. Ferrari-Dileo G, Davis EB, Anderson DR. Biochemical evidence for cholinergic activity in retinal blood vessels. *Invest Ophthalmol Vis Sci*. 1989;30:473–477.
54. Kur J, Newman EA, Chan-Ling T. Cellular and physiological mechanisms underlying blood flow regulation in the retina and choroid in health and disease. *Prog Retin Eye Res*. 2012;31:377–406.
55. Alarcon-Martinez L, Yilmaz-Ozcan S, Yemisci M, et al. Capillary pericytes express α-smooth muscle actin, which requires prevention of filamentous-actin depolymerization for detection. *Elife*. 2018;7:e34861.
56. Hughes S, Chan-Ling T. Characterization of smooth muscle cell and pericyte differentiation in the rat retina in vivo. *Invest Ophthalmol Vis Sci*. 2004;45:2795–2806.
57. Balaratnasingam C, Kang MH, Yu P, et al. Comparative quantitative study of astrocytes and capillary distribution in optic nerve laminar regions. *Exp Eye Res*. 2014;121:11–22.
58. Frank RN, Turczyn TJ, Das A. Pericyte coverage of retinal and cerebral capillaries. *Invest Ophthalmol Vis Sci*. 1990;31:999–1007.
59. Kornfield TE, Newman EA. Regulation of blood flow in the retinal trilaminar vascular network. *J Neurosci*. 2014;34:11504–11513.
60. Brozovich FV, Nicholson CJ, Degen CV, Gao YZ, Aggarwal M, Morgan KG. Mechanisms of vascular smooth muscle contraction and the basis for pharmacologic treatment of smooth muscle disorders. *Pharmacol Rev*. 2016;68:476–532.
61. Yu DY, Su EN, Cringle SJ, Morgan WH, McAllister IL, Yu PK. Local modulation of retinal vein tone. *Invest Ophthalmol Vis Sci*. 2016;57:412–419.
62. Kaizu Y, Nakao S, Arima M, et al. Capillary dropout is dominant in deep capillary plexus in early diabetic retinopathy in optical coherence tomography angiography. *Acta Ophthalmol*. 2019;97:e811–e812.
63. Dimitrova G, Chihara E. Implication of deep-vascular-layer alteration detected by optical coherence tomography angiography for the pathogenesis of diabetic retinopathy. *Ophthalmologica*. 2019;241:179–182.
64. Cao D, Yang D, Huang Z, et al. Optical coherence tomography angiography discerns preclinical diabetic retinopathy in eyes of patients with type 2 diabetes without clinical diabetic retinopathy. *Acta Diabetol*. 2018;55:469–477.
65. An D, Chandrasekera E, Yu DY, Balaratnasingam C. Nonproliferative diabetic retinopathy is characterized by nonuniform alterations to peripapillary capillary networks. *Invest Ophthalmol Vis Sci*. 2020;61:39.
66. de Oliveira F. Pericytes in diabetic retinopathy. *Br J Ophthalmol*. 1966;50:134–143.
67. Addison DJ, Garner A, Ashton N. Degeneration of intramural pericytes in diabetic retinopathy. *Br Med J*. 1970;1:264–266.
68. Cogan DG, Toussaint D, Kuwabara T. Retinal vascular patterns. IV. Diabetic retinopathy. *Arch Ophthalmol*. 1961;66:366–378.
69. Genevois O, Paques M, Simonutti M, et al. Microvascular remodeling after occlusion-recanalization of a branch retinal vein in rats. *Invest Ophthalmol Vis Sci*. 2004;45:594–600.
70. Freund KB, Sarraf D, Leong BCS, Garrity ST, Vupparaboina KK, Dansingani KK. Association of optical coherence tomography angiography of collaterals in retinal vein occlusion with major venous outflow through the deep vascular complex. *JAMA Ophthalmol*. 2018;136:1262–1270.
71. Rahimy E, Sarraf D, Dollin ML, Pitcher JD, Ho AC. Paracentral acute middle maculopathy in nonischemic central retinal vein occlusion. *Am J Ophthalmol*. 2014;158:372–380.
72. Rahimy E, Sarraf D. Paracentral acute middle maculopathy spectral domain optical coherence tomography feature of deep capillary ischemia. *Curr Opin Ophthalmol*. 2014;25:207–212.
73. Rahimy E, Kuehlewein L, Sadda SR, Sarraf D. Paracentral acute middle maculopathy: what we knew then and what we know now. *Retina*. 2015;35:1921–1930.
74. Krogh A. The number and distribution of capillaries in muscles with calculations of the oxygen pressure head necessary for supplying the tissue. *J Physiol*. 1919;52:409–415.
75. McLeod D. Misery perfusion, diffusive oxygen shunting and interarterial watershed infarction underlie oxygenation-based hypoperfusion maculopathy. *Am J Ophthalmol*. 2019;205:153–164.
76. Yu D-Y, Cringle SJ, Alder VA, Su EN. Intraretinal oxygen distribution in rats as a function of systemic blood pressure. *Am J Physiol*. 1994;36:H2498–H2507.

Investigative Ophthalmology & Visual Science